Optimization of Phase Change Material Heat Sinks for Low Duty Cycle High Peak Load Power Supplies

A. Stupar
U. Drofenik
J. W. Kolar

Optimization of Phase Change Material Heat Sinks for Low Duty Cycle High Peak Load Power Supplies

Andrija Stupar, *Student Member, IEEE*, Uwe Drofenik, *Member, IEEE*, and Johann W. Kolar, *Fellow, IEEE*

Abstract—A power electronic device's lifetime depends on its maximum operating temperature and the temperature swings it is subjected to. Heat sinks employing phase change materials (PCMs) can be employed to achieve a temperature reduction, but only for a limited duration. This makes such heat sinks appropriate for use in applications with high peak loads but with low duty cycles. The heat sink is modeled using the thermal resistors and capacitors (RCs) network approach, and an optimization procedure for designing a hybrid air-cooled heat sink containing PCM is developed, yielding a maximum possible temperature reduction for a given application. It is shown that air-cooled heat sinks employing pure PCMs are best suited for applications with pulses width lengths of several minutes with a period of several tens of minutes. In order to achieve a faster response of the PCM, the concept of PCM-metal foam is explored and modeled. Experimental data is presented which confirms the validity of the thermal RC network approach.

Index Terms—Cooling, modeling, power electronics, power supplies.

Nomenclature

k	Fin spacing ratio.
λ_{HS} (W/mK)	thermal conductivity of heat sink material.
A_{HS} (m^2)	Size of the heat sink base plate.
d_h (m)	Hydraulic diameter of one channel.
L (m)	Channel length in air flow direction.
n	Number of channels.
Δp (N/m^2)	Pressure drop in one channel.
V (m^3/s)	Volume flow.
Re_m	Average Reynolds number (for lam. or turb. flow).
Nu_m	Average Nusselt number (for lam. or turb. flow).
h (W/m^{2}K)	(Convective) heat transfer coefficient.
$Pr \approx 0.71$	Prandtl number (air, 80 °C).
$\rho_{AIR} \approx 0.99$ (kg/m^3)	Air density (80 °C).
$\nu_{AIR} \approx 2.1\text{e-}5$ (m^2/s)	Kinematic viscosity of the air (80 °C).
$c_{p,AIR} \approx 1010$ (J/kgK)	Specific thermal capacitance of air.
$\lambda_{AIR} \approx 0.03$ (W/mK)	Thermal conductivity of air (80 °C).

I. Introduction

POWER supplies having high peak loads yet low duty cycles are to be found in many up and coming applications. These are typically power electronics converters for systems which are inactive for relatively long periods of time and then need to suddenly burst into activity, such as electromechanical actuators in aircraft, namely retractors extenders for landing gear [1]. Such actuators are operated for several seconds during take-off and landing, and are then inactive for the duration of the flight, which can last several hours. Another application for which high peak low duty cycle power electronics can be used are novel ultracapacitor-powered electric buses [2], which recharge their batteries on certain stops, for 5 minutes, with 20 minutes in between charges. A generalized power profile representing applications as the above is shown in Fig. 1.

The reliability of such power converters, especially for transportation applications such as aerospace, is of great importance. Typically these power supplies are built using insulated-gate bipolar transistor (IGBT) modules. It has been shown [3], [4] that the peak operating temperature and the temperature cycle amplitude affect the lifetime of an IGBT module. It follows that the method of cooling, that is, the thermal management of power electronic devices, is of significant importance from the reliability standpoint.

One of the usual conventional approaches to cooling power electronic devices is to place them on an air-cooled finned metal heat sink with an attached fan. An alternative are hybrid heat sinks which employ phase change materials (PCMs) [6]–[9], as depicted in Fig. 2. In such configurations, the PCM absorbs heat as it changes from solid to liquid or liquid to gas, temporarily slowing the temperature rise of the device and resulting in a lower operating temperature over a certain period. PCM heat sinks are well suited for high peak load low duty cycle applications: the PCM absorbs the heat, lowering the device temperature, and then follows a long period of inactivity during which this absorbed heat can be released to the ambient. However, there are tradeoffs involved with this approach: while adding PCM increases the peak thermal capacity of the heat sink, it also significantly increases its thermal resistance.
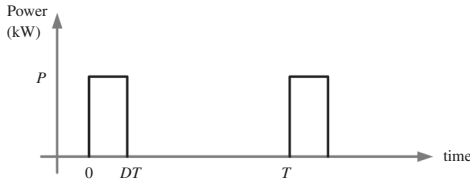
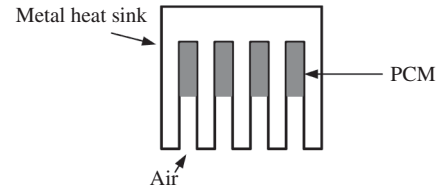Fig. 1.   Generalized high peak load low duty cycle power profile, with peak power P and period T much greater than on time DT.

Fig. 2.   Hybrid heat sink, with a portion of the channels filled with PCM (gray), and the rest free for air flow.

This paper presents an optimization procedure for designing a hybrid PCM-metal heat sink so as to arrive at a maximum reduction of the peak operating temperature compared to a conventional heat sink of equivalent volume. To achieve this, a thermal network model is developed, allowing for quick simulations and comparisons of different designs.

Section II of this paper briefly explains previous heat sink optimization work that it builds on. Section III discusses how the PCM is modeled, different possible configurations of the heat sink as well as material properties, and presents the optimization procedure, while Section IV gives its result for a particular example. In that section also the results given by the thermal network model are compared to results from 3-D-finite element method (FEM) simulations. Section V extends the model to a PCM-metal matrix in order to model a PCM-metal foam. Section VI presents experimental results and conclusions are given in Section VII.

II. OPTIMIZATION OF AIR-COOLED HEAT SINKS

This paper builds on previous work [10], [11] done for optimizing fan-cooled heat sinks. The optimization procedure for air-cooled heat sinks uses analytical and empirical equations and expressions for the air flow through the heat sink and the resulting thermal resistance of the heat sink, which is then minimized by varying the heat sink fin dimensions. The relevant parameters are shown in Fig. 3. A detailed discussion of the mathematical procedure and (1)–(14), and the accuracy of the theory verified by experimental results, can be found in [10] and [12]. This procedure and by extension this paper is limited to the commonly found heat sink shape shown in Fig. 3.

$$k = \frac{s}{b/n} \tag{1}$$

$$d_h = \frac{2s \cdot c}{s + c} \tag{2}$$

$$\Delta p_{lam}(V) = \frac{48 \, \rho_{AIR} \, \nu_{AIR} \, L}{n \, (s \cdot c) \, d_h^2} \, V \tag{3}$$

$$\Delta p_{turb}(V) = \frac{L \frac{s+c}{2s \cdot c} \, \rho_{AIR} \, \frac{1}{2} \left(\frac{V}{n \, (s \cdot c)} \right)^2}{\left(0.79 \cdot \ln \left(\frac{2V}{n \, (s+c) \nu_{AIR}} \right) - 1.64 \right)^2} \tag{4}$$

$$Re_m = \frac{2 \, V}{n \, (s + c) \, \nu_{AIR}} \tag{5}$$

$$k \cdot \Delta p_{FAN}(V) = \Delta p_{lam}(V_{lam}) \rightarrow V_{lam} \ \text{if} \ (Re_{m,lam} < 2300) \tag{6}$$
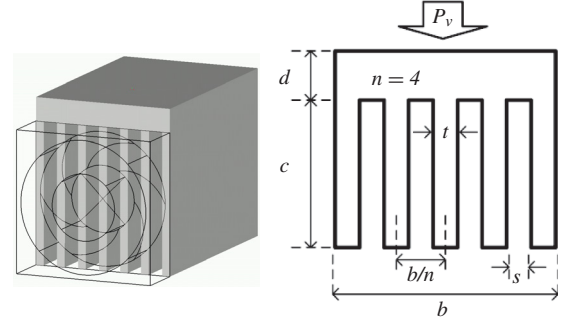

Fig. 3.   Air-cooled heat sink shape considered for optimization, with dimensions shown.

$$Nu_{m,lam}$$
$$= \frac{3.657 \left[\tanh \left(2.264 X^{\frac{1}{3}} + 1.7 X^{\frac{2}{3}} \right) \right]^{-1} + \frac{0.0499}{X} \tanh(X)}{\tanh \left[2.432 Pr^{\frac{1}{6}} X^{\frac{1}{6}} \right]} \tag{7}$$

$$X = \frac{L}{d_h \, Re_m \, Pr} \tag{8}$$

$$Nu_{m,turb}$$
$$= \frac{\{ 8 \cdot (0.79 \cdot \ln(Re_m) - 1.64)^2) \}^{-1} (Re_m - 1000) \, Pr}{1 + 12.7 \sqrt{\{ 8 \cdot (0.79 \cdot \ln(Re_m) - 1.64)^2) \}^{-1} \, (Pr^{\frac{2}{3}} - 1)}}$$
$$\cdot \left(1 + \left(\frac{d_h}{L} \right)^{\frac{2}{3}} \right). \tag{9}$$

The optimization procedure begins with the selection of a fan, which then defines the heat sink dimensions $b \times c$. The flow of air through the channels can be laminar or turbulent, with the pressure drop along the channel defined by (3) and (4), respectively. The air flow through the channels is found where (3) (for laminar flow) or (4) (turbulent) intersects with the pressure-flow fan characteristic obtainable from the fan datasheet. This is used to calculate the Reynolds number and (5) and (6) is used to determine whether the flow is laminar or turbulent – a Reynolds number less than 2300 indicates laminar flow. Knowing this, the appropriate Nusselt number can be calculated using (7) or (9). This allows then for the calculation of the heat transfer coefficient h (10). The transfer of heat from the heat sink surface to the air in one channel can be represented as a network of thermal resistors and capacitors (RCs), shown in Fig. 4.

For the optimization procedure, the capacitors are ignored. For geometries with $s << c$, $R_{th,a}$ is much greater than $R_{th,A}$ and can be ignored [10]. The rest of the resistances can be
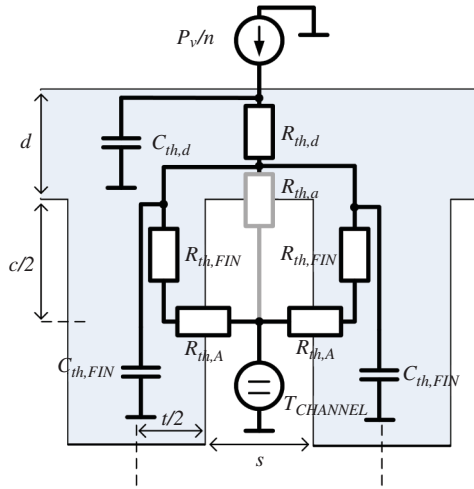
Fig. 4. Thermal resistor and capacitor network showing the heat flow through one channel of the heat sink.

TABLE I
THERMAL PROPERTIES OF PCMs AND ALUMINIUM

Material	ρ kg/m^3	λ W/mK	ΔH kJ/kg	T_{melt} °C	C_p J/kgK
Octadecane	774	0.35	244	28	-
Eicosane	785	0.15	247	36	2460
Heneicosane	788	0.15	213	40	-
Suntech P116	818	0.24	266	47	2730
Metallic alloy [6]	9160	15.0	14	47	147
PG (solid-solid)	750	0.17	177	83	2350
Aluminium	2700	210	–	–	903

phase transition is examined, while [14] deals with paraffin-water emulsions. Aluminium is chosen as the material for the metal part of the heat sink, its properties are also given in Table I.

The first parameter which is examined is the melting (i.e., phase change) temperature T_{melt}. Obviously the melting temperature should be above the ambient temperature; the change of phase is the heat absorption mechanism, and this should happen only after a power pulse is applied. The ambient temperature for this paper is selected as 45 °C (a typical industrial setting). This therefore removes from this investigation any PCMs with a lower T_{melt}, i.e., the first three materials in the table, and the paraffin-water emulsions of [14], which have T_{melt} in the range 0–20 °C. Furthermore it is advantageous to have the T_{melt} close to the ambient temperature, so that the phase change begins as soon as the power pulse is applied, so that heat is absorbed right away. Next, perhaps the parameter, of most interest, is the latent heat of melting ΔH, which specifies the heat absorbed during the change of phase. Of interest are also the density ρ and specific heat capacity C_p. Among the materials in Table I therefore, Suntech P116, which is a type of paraffin wax, is selected as it has a melting temperature close to but above the ambient, the highest latent heat, and a greater heat capacity-density product (i.e., heat capacity per volume) than the metallic alloy PCM or PG. Also note the low thermal conductivity λ of all the PCMs.

calculated using (10)–(13)

$$h = \frac{Nu_m \cdot \lambda_{AIR}}{d_h} \tag{10}$$

$$R_{th,A} = \frac{1}{h \cdot L \cdot c} \tag{11}$$

$$R_{th,FIN} = \frac{\frac{1}{2}c}{\frac{1}{2}t \cdot L \cdot \lambda_{HS}} \tag{12}$$

$$R_{th,d} = \frac{d}{\frac{1}{n} A_{HS} \lambda_{HS}} \tag{13}$$

$$R_{th,S-a}^{(HS)} = \frac{1}{n}\left(R_{th,d} + \frac{1}{2}(R_{th,FIN} + R_{th,A})\right) + \frac{0.5}{\rho_{AIR} c_{P,AIR} V}. \tag{14}$$

Equation (14) gives the total thermal resistance of the heat sink. The term on the right represents the average temperature rise of the air in the channel due to the heat transported away by convection. The optimization procedure therefore consists of varying the dimensions s and t (or one of those and the number of channels n), for a given fan, until the minimum total thermal resistance, calculated using (1)–(14), is found. Note that this model assumes that there is no air flow over the fin tips of the heat sink, i.e., that the heat sink is in an enclosure, "closed" on both the top and bottom side. Air enters only via the fan into the heat sink channels, and exits through the opposite side, flowing only through the channels.

III. OPTIMIZATION OF HYBRID PCM HEAT SINKS

To arrive at an optimization procedure for a hybrid heat sink which is both air-cooled and contains PCM, the method of Section II is extended to include the effects of the PCM. Therefore, a corresponding thermal network must be found. To start, first the properties of the material are considered.

A. PCM Properties

The properties of some PCMs commonly cited in literature [5]–[7], [9], [13], [14] are given in Table I. In [5]–[7], and [9] PCMs which change phase from solid to liquid are investigated, in [13] pentaglycerine (PG) undergoing a solid-solid

B. Modeling the PCM

Mathematical models of PCMs are well-established and experimentally verified [7]–[9], [13]–[15]. Adopted here is the variable specific heat capacity approach of [9], [13], and [15]. Essentially, the specific heat capacity of the PCM increases by $\Delta H / \Delta T$, where ΔT is the temperature range over which the PCM melts. In [9] it is shown that a realistic range is $\Delta T = 3$ °C. Therefore the apparent heat capacity [9] of the PCM, C_{app}, can be defined as

$$C_{app} = \begin{cases} C_p, & \text{for } T \leq T_{melt} \\ C_p + \frac{\Delta H}{\Delta T}, & \text{for } T_{melt} < T < T_{melt} + \Delta T \\ C_p, & \text{for } T \geq T_{melt} + \Delta T. \end{cases} \tag{15}$$

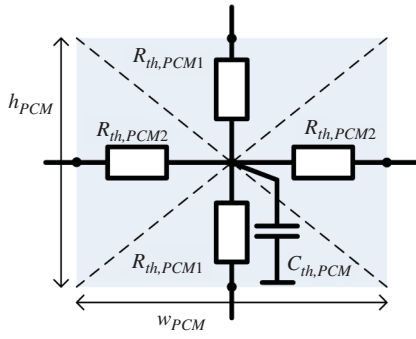As in [6] and [7], to simplify the modeling, all the other material properties are assumed constant over the entire

Fig. 5. Thermal resistor and capacitor network model of rectangular volume of PCM.
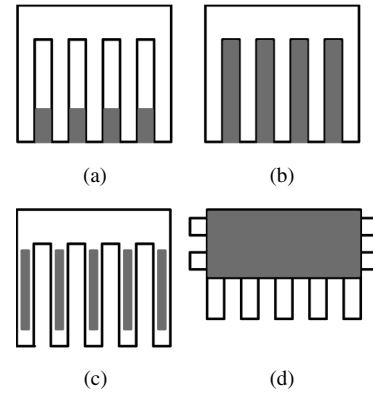

Fig. 6. Different combinations of PCM heat sinks found in literature, PCM shown in gray. (a) Heat sink fins tip immersed in PCM. (b) PCM completely filling heat sink channels. (c) PCM embedded in heat sink fins. (d) Large PCM compartment surrounded by fins.

temperature range under consideration. The effect of the molten material flowing can also be ignored [6], [7]. Using the material properties, a thermal network model of a single PCM block is developed, shown in Fig. 5. A rectangular volume of PCM is divided into four equivalent thermal resistors (conduction from all sides) with a single thermal capacitor for the entire volume placed in the midpoint. Equations (16)–(18) give the definitions for the elements of the thermal circuit in Fig. 5. The dimensions h_{PCM}, w_{PCM}, and l_{PCM} are the height, width, and length of the PCM block, respectively, and λ_{PCM} and ρ_{PCM} are the thermal conductivity and density of the material, respectively

$$R_{th,PCM1} = \frac{\frac{1}{2} h_{PCM}}{\frac{1}{2} w_{PCM} \cdot l_{PCM} \cdot \lambda_{PCM}} \quad (16)$$

$$R_{th,PCM2} = \frac{\frac{1}{2} w_{PCM}}{\frac{1}{2} w_{PCM} \cdot l_{PCM} \cdot \lambda_{PCM}} \quad (17)$$

$$C_{th,PCM} = h_{PCM} \cdot w_{PCM} \cdot l_{PCM} \cdot \rho_{PCM} \cdot C_{app}. \quad (18)$$

C. Different PCM Heat Sink Configurations

Different heat sink configurations are found in literature [5]–[9], [13]–[16]. The most common approaches are shown in Fig. 6. In [5], [13], [17], and [18] optimization techniques for the configuration of Fig. 6(b) are presented. In this configuration there is no airflow between the fins, and the procedure of Section II therefore cannot be applied; also, this configuration is characterized by a large thermal resistance due to the PCMs low conductivity, and a very slow ejection of heat to the ambient once the power pulse has passed, since there is no fan and associated forced air flow. For these reasons, the configuration of Fig. 6(b) is not considered further in this paper. The configuration of Fig. 6(c) is the topic of [16], where the PCM is embedded in the heat sink fins. The optimization procedure of Section II tends to produce fin thicknesses in the order of a few millimetres. With that in mind, the configuration of Fig. 6(c) would be very difficult (if not impossible) to manufacture, and it is therefore not considered further. This leaves configurations Fig. 6(a) [7], where the tips of the fins are immersed in PCM, and Fig. 6(d) [6], where the heat source is placed on top of a large PCM-filled compartment. The advantage of the latter is the PCM is close to the heat source, allowing for quick heat absorption. The disadvantage is that the thermal resistance of such a heat sink from heat source to the ambient air is very high, due

to the low thermal conductivity of the PCM, meaning that the heat sink performance degrades greatly as compared to a regular heat sink once the PCM is melted. The advantage of the former is that a large section of the heat sink can be left open for air flow, with a thermal resistance from heat source to the air comparable to that of a conventional heat sink. The disadvantage is that the PCM is farther from the heat source, and so it takes longer for the heat to reach it.

1) Selected Heat Sink Configuration: An obvious approach is then to somehow combine the advantages of the configurations of Fig. 6(a) and (d). Analyzing from the perspective of the thermal networks in Figs. 4 and 5, and keeping in mind the properties of the materials, the following design guidelines become clear.

1) Since $\lambda_{PCM} \ll \lambda_{HS}$, we have $R_{th,PCM1} \gg R_{th,d}$, and therefore there should be a path of metal from the heat source to the fins; in this way, once the PCM is melted, heat can flow from the heat source to the ambient effectively bypassing the high-resistance PCM.

2) The results of optimizations of PCM-metal heat sinks from [5], [13], [17], and [18] show that the PCM should not be one monolithic block, but divided into several cells surrounded by metal, as to improve the heat transfer into and out of the material.

3) The $C_p \cdot \rho$ product, i.e., the heat capacity per volume, is greater for aluminium than for the chosen PCM, meaning that outside of the phase transition, the PCM will have a lower thermal capacitance than an equivalent volume of the metal. This suggests that replacing air with PCM is preferable to replacing metal with PCM, as the former increases resistance but also capacitance, while the latter increases resistance and decreases the capacitance (outside of the phase transition). Furthermore, as discussed in [10], decreasing base plate thickness d decreases the heat spreading effect of the base plate, which is undesirable.

4) The thermal resistance between the heat source and the PCM should be minimized.

Following these guidelines, the resulting heat sink configuration is one where the base plate is unmodified and the

PCM is placed between the fins, but moved closer to the heat source – it is placed at the beginning of the fins, right after the base plate, rather than at the fins. This is the configuration shown in Fig. 1, and also in more detail in Fig. 7(a).

2) PCM Heat Sink Thermal Network: The thermal network for one channel of the selected heat sink configuration is given in Fig. 7(b). Equations (19)–(24) give the expressions for the elements of the network. Terms not defined here are the same as in Section II. The resistor from the PCM to the ambient is ignored for the same reason as $R_{th,a}$ in Section II

$$R_{th,FIN-PCM} = \frac{\frac{1}{2}c_{PCM}}{\frac{1}{2}t \cdot L \cdot \lambda_{HS}} \quad (19)$$

$$C_{th,d} = \frac{1}{n}A_{HS} \cdot \rho_{HS} \cdot C_{HS} \quad (20)$$

$$C_{th,d} = \frac{1}{2}t \cdot L \cdot s \cdot \rho_{HS} \cdot C_{HS} \quad (21)$$

$$R_{th,PCM1} = \frac{\frac{1}{2}c_{PCM}}{\frac{1}{2}s \cdot L \cdot \lambda_{PCM}} \quad (22)$$

$$R_{th,PCM2} = \frac{\frac{1}{2}s}{\frac{1}{2}c_{PCM} \cdot L \cdot \lambda_{PCM}} \quad (23)$$

$$C_{th,PCM} = s \cdot c_{PCM} \cdot L \cdot \rho_{PCM} \cdot C_{app}. \quad (24)$$

The dimension c is the height of the channel exposed to air flow, while c_{PCM} is the height of the channel filled with PCM, and ρ_{HS} and C_{HS} are the density and specific heat capacity of the metal.

D. Optimization Procedure

Due to the tradeoffs involved with adding PCM to a heat sink, it is not simply enough to optimize for a final stationary thermal resistance as in Section II. Adding PCM increases thermal resistance, but also adds a large variable capacitance. Whether a particular PCM heat sink is useful for a pulsed-power application therefore depends on the transient properties of the heat sink and the characteristics of the power pulse – its amplitude and duration. Therefore, to compare heat sinks with varying amounts of PCM, simulations of the response of the heat sink thermal RC network to the pulse must be performed. In this way, different variations can be compared and the optimum dimensions chosen. The optimization procedure of Section II can be performed on a computer in seconds. The simulation of a derived thermal RC network can also be performed in seconds with the help of a circuit simulator. If that is compared to the significantly longer simulation times needed to simulate heat sink structures in 3-D-FEM simulators, the advantage of the thermal RC model approach becomes apparent.

The optimization procedure can be then broadly described by the following steps.

1) Pick a set of heat sink dimensions.
2) Use the equations of Sections II and III-B2 to derive the thermal network of the heat sink.
3) Obtain the response of the network to the desired power pulse.
4) Repeat steps 1–3 until all variations are exhausted.
5) Compare responses and pick the heat sink with the greatest temperature reduction.
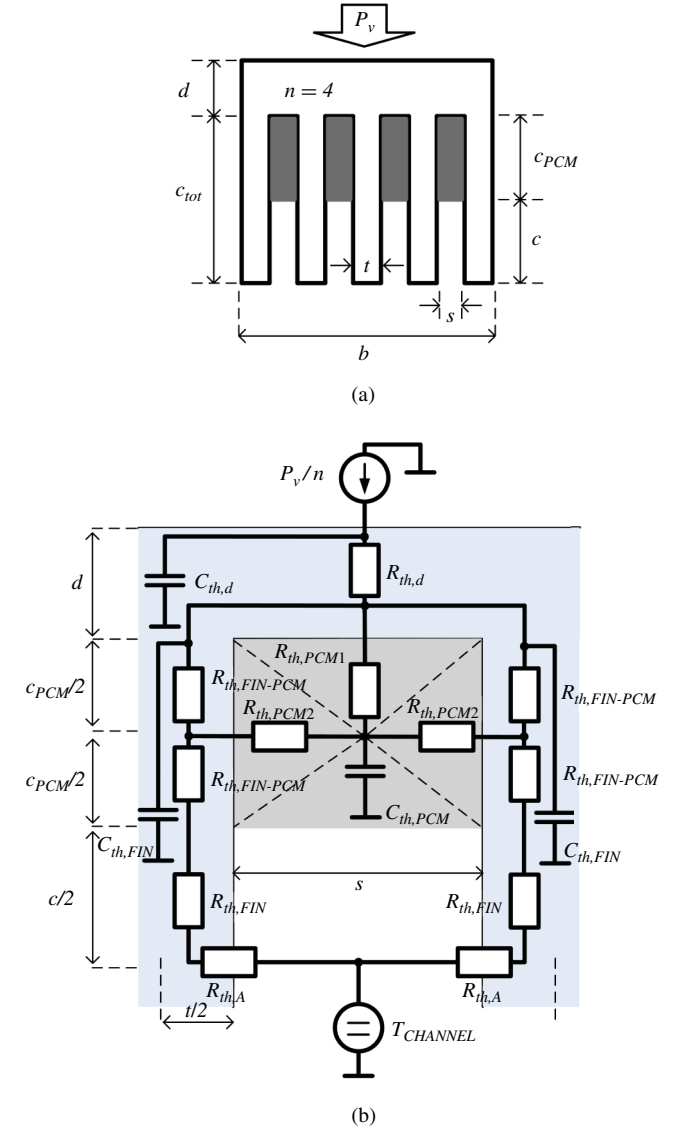

(a)

(b)

Fig. 7.　(a) Chosen hybrid PCM heat sink configuration with dimensions shown. (b) Thermal resistance and capacitance network showing the heat flow through one channel of the PCM heat sink.

The following sections explain the optimization procedure in more detail.

1) Full Optimization: The method of Section II varies the heat sink fin thickness and the number of channels until the minimum thermal resistance is achieved with a given fan (and thus air flow). With the heat sink where PCM is added in between the fins, the varying of these parameters also affects the volume of PCM added to the heat sink. A complete optimization procedure would then vary the parameters c_{PCM}, t, and n, and compare the response of each variation until an optimum is found. However, this would require simulating and comparing a very large number of possible geometries. For this reason, this approach is not undertaken in this paper. Moreover, as noted in [10], the optimization procedure of Section II tends to produce thin fins and generally $s > t$, so often the theoretical optimum is very difficult or impossible to manufacture. For this reason, the assumption is made that the

PCM cell width s is near the optimum of what is physically producible for any channel width s given as optimal by the procedure in Section II.

2) Partial Optimization: The approach taken in this paper therefore is to optimize the parameters n, s, and t for a given area $b \times c$. First, $b \times c$ is defined by the chosen fan and c_{PCM} is set to zero to obtain an optimized conventional heat sink. Then c_{PCM} is incremented by an amount, and correspondingly c is decremented by the same amount. The new optimal set of parameters n, s, and t is then found for the new area $b \times c$, using the method of Section II. The procedure is repeated until the channels are fully filled with PCM (this last variation is discarded as there is no air flow). At each step the thermal network is calculated; the responses of the networks are then compared to obtain the optimum dimensions.

Note that each time PCM is added, the available area for air flow decreases. The assumption made during this optimization procedure is that the fan however remains fully utilized; i.e., all the air which would be forced through the conventional heat sink area $b \times c_{tot}$ is forced through the reduced areas $b \times c$ for each variation of the PCM amount. Instead of the portion of the fan facing the PCM simply being blocked, an air guide or duct can be constructed to direct all the air into the reduced area. It is assumed that if this duct is constructed with a mild slope (no abrupt bends) and of a low resistance material (i.e., a smooth plastic) then no significant pressure loss compared to the heat sink without PCM occurs. Note the reduced area changes the optimal fan operating point, and that finding this operating point is done in this optimization as in the conventional heat sink optimization described in Section II.

3) Optimizing the Amount of Added PCM: A simpler approach that may be of practical interest is to simply add PCM to the conventional heat sink, i.e., vary c_{PCM} but without re-optimizing the remaining parameters at each step. This may be useful in a situation where for example the power system designer wishes to improve the performance of a commercially available heat sink by adding PCM, which can be purchased separately.

IV. OPTIMIZATION EXAMPLE

A particular optimization scenario, with results, is presented in this section. Also, the results obtained are compared with a 3-D-FEM simulation of the PCM heat sink performed using the *Icepak* software.

A. Power Profile

As the optimization procedure is application-specific, high peak power low duty cycle applications such as those mentioned in Section I were examined. Power electronic devices that are suitable for such applications and their losses dissipated to the heat sink as heat were investigated. The heat sink dimensions $L \times b$ were chosen as to have the power electronics module cover the entire area of the heat sink. A loss per area of the heat sink figure of 5 W/cm^2 was found to be an adequate representation of a range of applications and appropriate modules.

TABLE II
CONVENTIONAL HEAT SINK (OPTIMIZED WITHOUT PCM)
DIMENSIONS (mm)

b	c	L	n	s	t
60	60	110	18	2.3	1.0

B. Conventional Heat Sink without PCM

The dimensions $L = 110$ mm and $b = 60$ mm were chosen, giving a heat sink area that can accommodate several kinds of commercial IGBT modules. An according fan with dimensions $b = c = 60$ mm was then chosen, in this case the Sanyo Denki *9WP0612H402* [19]. The minimum fin thickness was set at $t = 1.0$ mm, to reflect a heat sink that can realistically be manufactured. Using the procedure of Section II, the optimized conventional heat sink was found with $n = 18$, $s = 2.3$ mm, and $t = 1.0$ mm.

Using the previous figure for losses of 5 W/cm^2, the heat sink area gives a power pulse with an amplitude of 330 W. The heat sink dimensions are summarized in Table II.

C. Optimized Heat Sink Dimensions with PCM Included

The method of Section III-D2 was applied: in this case c_{PCM} was first incremented by 5 mm from 0 to 55 mm. The diminishing available area for air flow was then re-optimized at each step. As c_{PCM} was increased, the optimization routine gave smaller and smaller fin thickness t, decreasing to below 1.0 mm. When the thickness was limited to a manufacturable 1.0 mm as in the previous section, at each step the optimization yielded either the same dimensions as the conventional heat sink, or a very similar configuration of $n = 19$, $s = 2.1$ mm, and $t = 1.0$ mm. For this reason, the simpler method of Section III-D3 was used for the next steps: only the amount of PCM was varied while the other dimensions were kept the same as in Table II.

D. Comparison with 3-D-FEM Simulations

A common but often time consuming way of modeling and simulating thermal systems is via 3-D finite-element solvers. As an initial check of the validity of the model described in this paper, the output of the thermal network was compared to 3-D simulations of the hybrid PCM heat sink. As in [10], there is a difference of approximately 20% compared to the results using the thermal network. Also as in [10], the overall thermal resistance calculated by the thermal model is greater than that obtained through 3-D-FEM simulation. An error is to be expected since the many hundreds or thousands of simulated cells of a 3-D simulation are reduced by the thermal network model to only a few cells, and because of the many approximations of the analytical expressions (see [10]). It should be noted also that in [10], where the method of Section II is derived and verified experimentally, the experimental measurements yielded values in between, less than those given by the thermal network model but greater than derived from the 3-D simulation.

Although there is a difference between the absolute numerical values of the two simulations, the general behavior of the
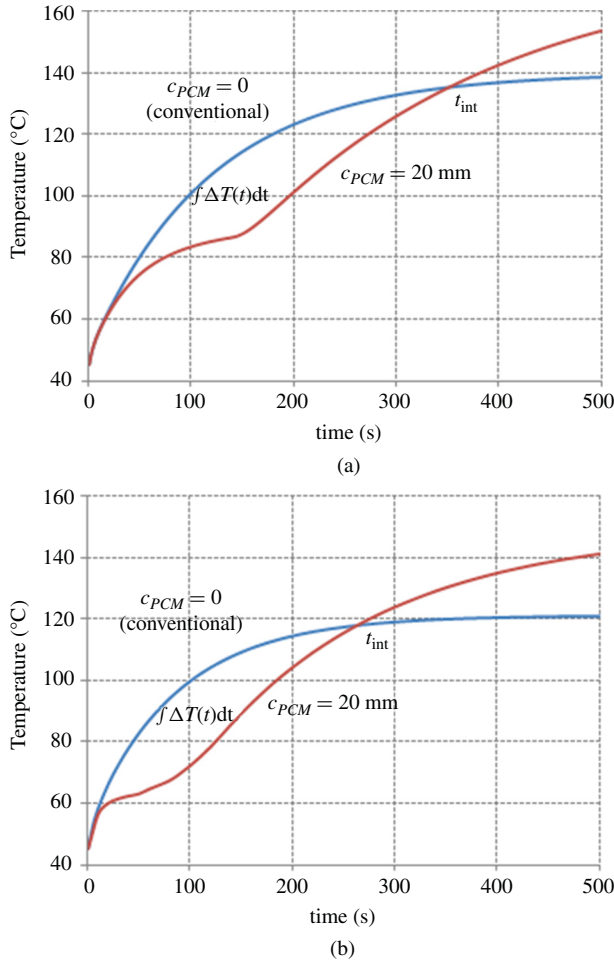
Fig. 8. Response to a 330 W step, heat sinks with no PCM and with a third of the channel length filled with PCM. (a) Thermal RC network simulation. (b) Icepak simulation.

TABLE III
COMPARISON OF THE RELATIVE IMPROVEMENT GAINED BY ADDING PCM TO A HEAT SINK FROM TWO DIFFERENT SIMULATIONS

	Thermal network	3-D-FEM
$R_{th,S-a}^{(HS)}$, $c_{PCM} = 0$ (K/W)	0.29	0.23
Q_I	0.117	0.152
Temp. (°C) at $t = 120$ s, $c_{PCM} = 0$	107	104.2
Temp. (°C) at $t = 120$ s, $c_{PCM} = 20$ mm	85.7	78.4
ΔT at $t = 120$ s	21.3	25.8
Temp. reduction compared to $c_{PCM} = 0$ (%)	19.9	24.8

Fig. 9. Response to a 330 W pulse of duration 120 s of heat sinks with varying amounts of PCM.

curves is the same. The step responses of the conventional heat sink and a heat sink with one third of the channel height filled with PCM ($c_{PCM} = 20$ mm) to a 330 W step from both the thermal network model and 3-D model are given in Fig. 8.

In order to quantify the transient performance of the PCM heat sink for comparison between the two simulations, the area under (i.e., the integral of) the step-response curve for the conventional heat sink $\int T(t)dt$ is considered. The area in between the two curves, the curve for the conventional heat sink with no PCM and for the heat sink with PCM, $\int \Delta T(t)dt$, can then be thought of as a reduction of the original area $\int T(t)dt$, allowing for the definition of a relative improvement index Q_I

$$Q_I = \frac{\int_0^{t_{int}} \Delta T(t)dt}{\int_0^{t_{int}} T(t)dt}. \tag{25}$$

The absolute temperature reduction ΔT at a given time of the PCM heat sink compared to the conventional heat sink is also compared. These values are summarized in Table III. Again, the values differ by approximately 20%. Compared to the 3-D-FEM simulations, it can be said the thermal network model underestimates the improvement gained by adding PCM. It is clear the thermal network modeling approach is a good guideline for optimizing hybrid PCM heat sinks.

E. Optimization Results

Adding PCM to the heat sink increases its thermal resistance, that is why once the PCM is melted, the temperature of the PCM heat sink surfaces exceeds that of the conventional heat sink, assuming a constant power input, as can be seen in Fig. 8. Therefore there is a certain range, or power pulsewidth, over which the PCM heat sink is useful. The re-solidification of the PCM during which it ejects the heat to ambient must also be taken into consideration: if the PCM does not re-solidify by the time the next power pulse arrives, the advantages of the phase change heat absorption mechanism will not be utilized. Therefore, a specific load period and duty cycle must be selected. Note from Fig. 8 the slow response (tens to hundreds of seconds) of the PCM: the hybrid heat sink confers no advantage to situations where the pulse is only several seconds long or shorter. To complete the procedure consider for example the application of an ultracapacitor powered road vehicle (similar to [2]) which can recharge its capacitors in 2 minutes and go 45 minutes between charges. The response to the corresponding pulse of 330 W, period 2700 seconds, duty ratio 0.044 (120 seconds) is given in Fig. 9.
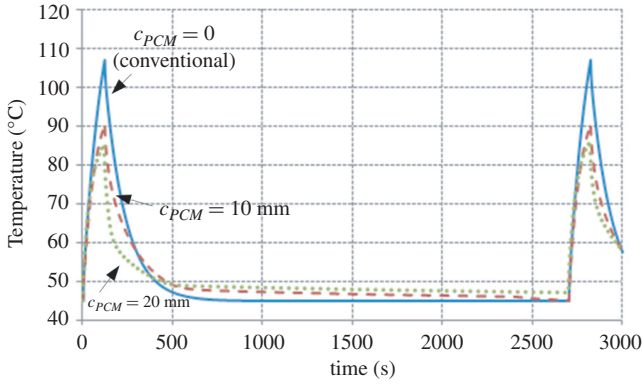
Fig. 10. Response to two consecutive pulses of the conventional heat sink (solid line), $C_{PCM} = 10$ mm (dashed) and $C_{PCM} = 20$ mm (dotted).
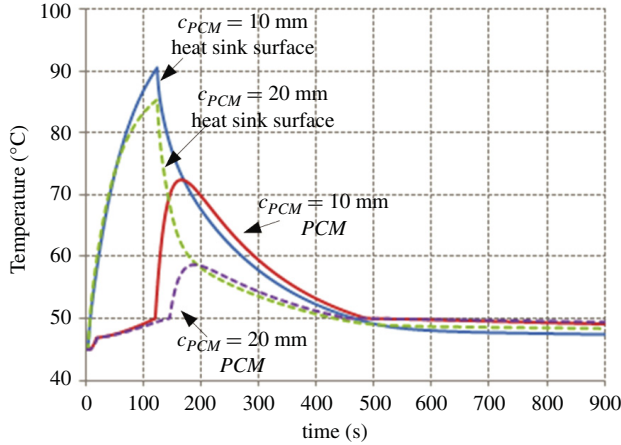

Fig. 11. Temperature of the heat sink surface and of the PCM itself during the pulse for $C_{PCM} = 10$ mm (solid line) and $C_{PCM} = 20$ mm (dashed). Note the larger difference between the two temperatures when there is more PCM.

TABLE IV

PERFORMANCE OF DIFFERENT HEAT SINK CONFIGURATIONS WITH VARYING AMOUNTS OF PCM: THE FIRST PULSE AT 120 s, THE END OF PERIOD AT 2700 s, AND THE SECOND PULSE AT 2820 s

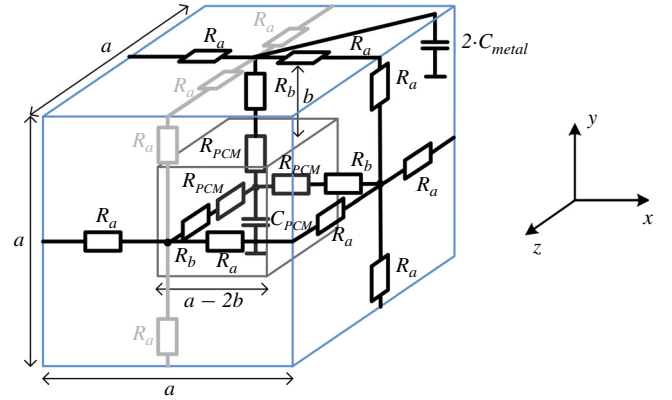|	Temperature (°C)		
PCM (mm)	$t = 120$ s	$t = 2700$ s	$t = 2820$ s
$c_{PCM} = 0$	106.3	45.0	106.3
$c_{PCM} = 10$	90.1	45.2	90.1
$c_{PCM} = 20$	85.1	47.0	85.7
$c_{PCM} = 30$	83.3	47.7	84.6
$c_{PCM} = 40$	83.4	48.0	84.7
$c_{PCM} = 50$	84.7	48.3	86.3

Fig. 12. Model of an element of a PCM-metal matrix, or foam outer cube of metal and inner cube of PCM. The resistors in light gray are ignored for the purpose of further modeling. Heat from cube-to-cube flows only through the side faces in the x direction – from the fins into the PCM.

Fig. 9 shows the first 200 s of the period, with the peak temperature for configurations with $0 \leq c_{PCM} \leq 50$ mm, varied at 10 mm increments. As PCM is added, the peak temperature is reduced. From this it might seem that the configuration with the most PCM should be selected; however, the re-solidification phase must also be examined. Also, it is not clear how well the fan assumption of Section III-D2 holds with the available area for air flow reduced by more than two-thirds.

Note that from Fig. 9 it would appear that the heat sinks with more PCM cool more quickly. As seen in Fig. 10 however, which shows two pulses, this is only a temporary effect, which can be explained by examining Fig. 11, showing the temperature of the heat sink surface as well as of the PCM. The more PCM is added, the higher the capacity of the PCM, the higher the thermal resistance between the PCM and the metal, and therefore the higher the temperature difference between the heat sink surface and the PCM. Hence the initial decoupling: the metal, being hotter, first cools down to the temperature of the PCM, and then the two continue to cool at a slower rate. Eventually the heat sinks with less PCM settle down to a lower temperature than those with more. The same behavior is seen in 3-D simulations.

Table IV summarizes the performance of the configurations. As can be seen, only the configuration with $c_{PCM} = 10$ mm re-solidifies in time for the next pulse, while all the others are still partly molten at that point, and so their peak temperatures during the second pulse are higher than in the first. Therefore, the configuration $c_{PCM} = 10$ mm is selected as the optimum heat sink for this application. Compared to the conventional heat sink, the peak temperature is reduced by 16 °C.

To justify the assumption of Section IV-C above, an example is provided of a "true" optimum heat sink with $c_{PCM} = 10$ mm, i.e., with arbitrary fin thickness t below 1.0 mm. The optimization routine then returns $n = 26$, $s = 1.7$ mm, $t = 0.5852$ mm. Such a heat sink is not easily realistically manufacturable.

V. PCM-METAL FOAM

As can be seen from Fig. 11, in the heat sink described in the previous sections, it takes about 15 s for the PCM to begin to melt, and as seen in Fig. 8, at least approximately 20 s for the effect of this phase transition to become visible on the heat sink surface. This is due to the low thermal conductivity of PCM materials (see Table I). The result is that such heat sinks are useful for achieving noticeable peak temperature reductions only in applications where power pulse lengths are on the time scale of several tens to hundreds of seconds, i.e.,
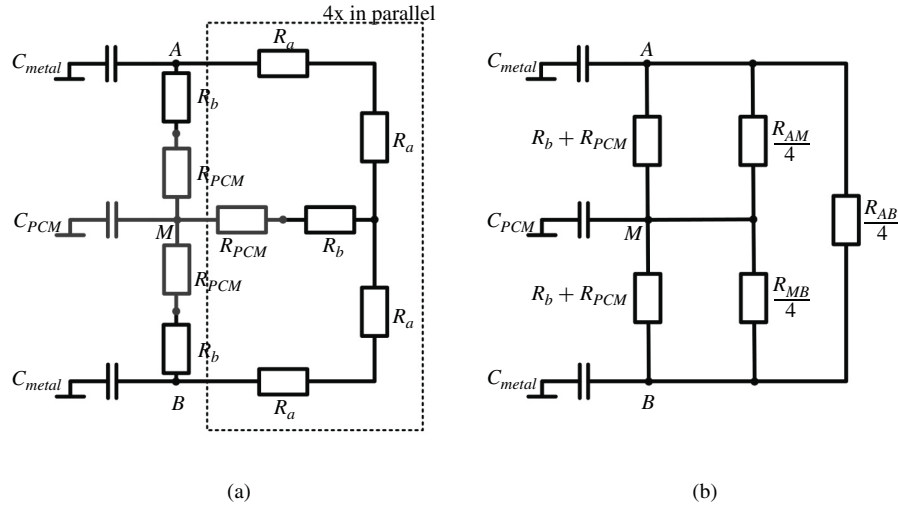
Fig. 13. (a) Thermal RC network of the PCM-metal cube of Fig. 12. The metal capacitance is split into two capacitors to ease simplification of the network. The part of the network inside the dotted box repeats four times, connected in parallel between points A, B, and M. (b) Network of the cube after a $Y - \Delta$ transform is applied to the portion inside the dotted box, replacing those six resistors by equivalent resistors R_{AM}, R_{AB}, and R_{MB}, which are then divided by four to reduce the four parallel branches of the network into one.

on the scale of minutes. A faster melting PCM is required if the heat sinks discussed in this paper are to be useful in applications with shorter pulses. One way to achieve this, that is, to mitigate the low thermal conductivity of PCM, is to embed it in a matrix of high conductivity material, as done in [15] with PCM-filled carbon foam. This creates a large number of high-conductivity paths within the PCM, allowing the heat to reach more of the PCM more quickly, thus melting it faster.

A. PCM Foam Model

One element of such a matrix, or foam, can then be modeled as a cube of metal (high conductivity) inside of which there is another cube of PCM (low conductivity), as shown in Fig. 12. The RC thermal network of such an arrangement is given by (26)–(30). For simplicity and brevity, a direct coupling between the PCM and metal thermal resistances is assumed, although there is in reality an additional thermal resistance between them, governed by an interstitial heat transfer coefficient which limits heat conduction between the two materials, as discussed in detail in [20] and [21]. Consider then a PCM placed inside a heat sink channel, in between two fins as in Fig. 7, consisting of a number of such cubes stacked one next to and on top of one another. For the heat sink selected through the optimization procedure of Section IV with $c_{PCM} = 10$ mm, the width (2.3 mm) of such a PCM "slab" is more than four times smaller than the height (10 mm), creating a much larger thermal resistance at the interface of the PCM with the heat sink base plate compared the resistance at the interface of the PCM with the heat sink fins. Looking at Fig. 7(b), and (22) and (23), $R_{th, PCM1}$ is approximately 19 times greater than $R_{th, PCM2}$ in this case. Therefore almost all of the heat flows to the PCM via the fins, and to simplify the modeling of the PCM foam the interface between the base plate and the PCM is ignored. It follows then that the heat flow in the z direction on the top and bottom faces of the
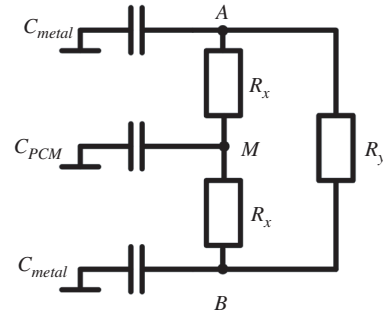

Fig. 14. Simplified model of the cell of Fig. 12 after applying standard RC network transformations.

cube and in the y direction on the front and back faces of the cube is ignored, with the associated R_a resistors (shown in gray in Fig. 12), and that only heat flow in the x direction from cube to cube is considered. This allows the double cube of Fig. 12 to be represented by the RC network of Fig. 13(a)

$$R_a = \frac{a}{\lambda_{metal} \cdot b} \tag{26}$$

$$R_b = \frac{b}{\lambda_{metal} \cdot (a - b)^2} \tag{27}$$

$$R_{PCM} = \frac{1}{\lambda_{PCM} \cdot \left(\frac{a}{2} - b\right)} \tag{28}$$

$$C_{metal} = \frac{1}{2}\left[a^3 - (a - 2b)^3\right] \cdot \rho_{metal} \cdot C_{Pmetal} \tag{29}$$

$$C_{PCM} = (a - 2b)^3 \cdot \rho_{PCM} \cdot C_{PPCM}. \tag{30}$$

This circuit can be further simplified by adding the resistors which are in series, R_a and R_a as well as R_b and R_{PCM}, cutting the number of resistors in the network in half. Furthermore, a Υ-Δ transform (31)–(33) is performed on the Υ (star) portion of the network connected four times in parallel to the points A, M, and B, resulting in three thermal resistors R_{AM}, R_{MB}, and R_{AB} connected between those three points
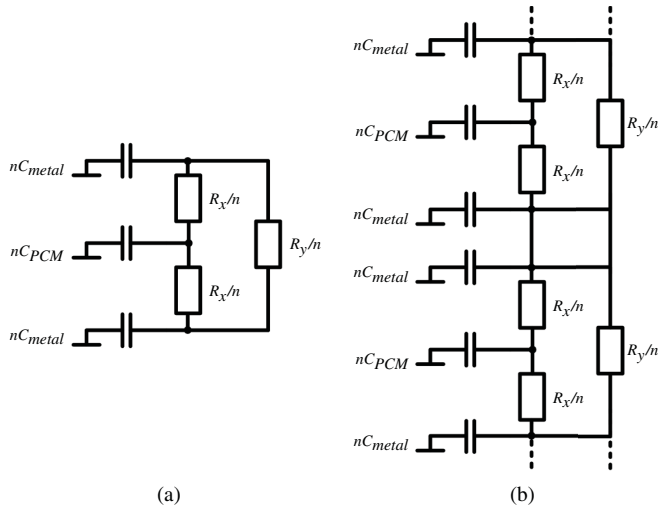
(a) (b)

Fig. 15. (a) Model of n cells of Fig. 12 connected in a plane in parallel. (b) Model of a 3-D stack of cells.

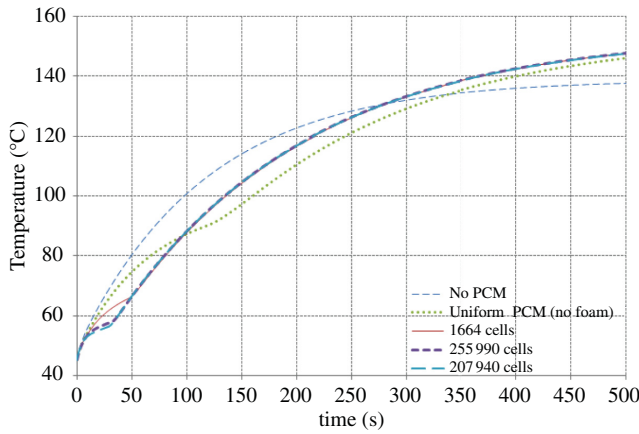Fig. 17. Temperature of the PCM of different PCM-metal matrix combinations, during a 330 W step.

Fig. 16. Response of different PCM-metal matrix combinations, all 50% PCM 50% metal, to a 330 W step. All of the variations with PCM eventually converge to the same value.

Fig. 18. Response of a 207 940 per channel cell PCM-foam matrix with varying amounts of PCM to a 330 W step.

in a Δ (triangle) configuration. This allows the four parallel portions of the network to be easily simplified, giving finally the network of Fig. 13(b)

$$R_{AM} = \frac{2R_a \cdot (R_b + R_{PCM}) + (R_b + R_{PCM}) \cdot 2R_a + 2R_a \cdot 2R_a}{2R_a}$$
$$= 2 \cdot (R_a + R_b + R_{PCM}) \tag{31}$$
$$R_{MB} = \frac{2R_a \cdot (R_b + R_{PCM}) + (R_b + R_{PCM}) \cdot 2R_a + 2R_a \cdot 2R_a}{2R_a}$$
$$= R_{AM} \tag{32}$$
$$R_{AB} = \frac{2R_a \cdot (R_b + R_{PCM}) + (R_b + R_{PCM}) \cdot 2R_a + 2R_a \cdot 2R_a}{(R_b + R_{PCM})}$$
$$= 4R_a \cdot \left(1 + \frac{R_a}{R_b + R_{PCM}}\right). \tag{33}$$

Reducing the parallel resistors between points A and M, and M and B in Fig. 13(b) into one results in the simplified RC network of Fig. 14 for the PCM-metal cube, with resistors R_x
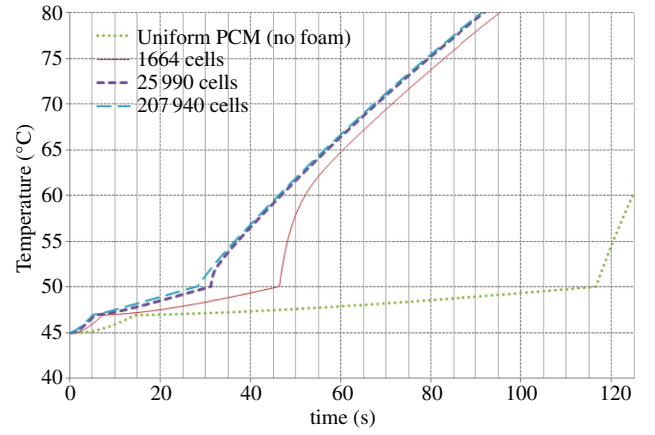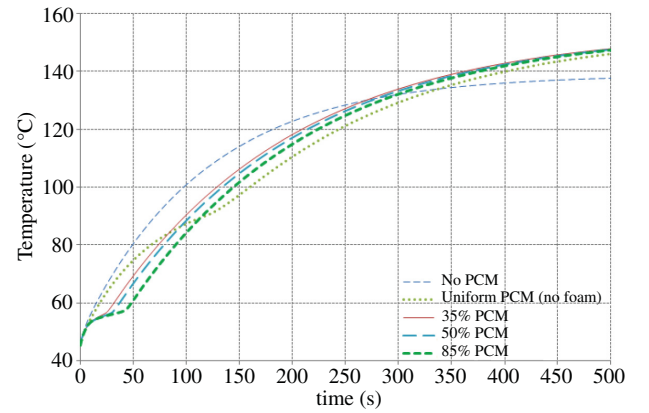
and R_y as given by (34) and (35)

$$R_x = (R_b + R_{PCM}) || \frac{R_{AM}}{4}$$
$$= \left(\frac{1}{R_b + R_{PCM}} + \frac{2}{R_a + R_b + R_{PCM}}\right)^{-1} \tag{34}$$
$$R_y = \frac{R_{AB}}{4} = R_a \cdot \left(1 + \frac{R_a}{R_b + R_{PC}}\right). \tag{35}$$

Fig. 15(a) then gives the RC network of a vertical plane of n such cubes connected in parallel. To obtain finally the 3-D model of a PCM-metal foam structure, a number of such planes are stacked next to one another, with the RC networks connected as in Fig. 15(b). The number of planes, and therefore the size of the network, depends on the cube dimensions – the smaller the cubes, the larger the RC network modeling the foam. To model a heat sink containing such foam between the fins in place of uniform PCM (as in Fig. 2), the RC network of Fig. 15(b) replaces the network of Fig. 5 in Fig. 7(b).

B. PCM Foam Performance

The PCM used for the foam model was Suntech P116, as in the previous sections. Investigated first was the effect of

TABLE V

PARAMETERS OF THE STEP RESPONSES OF HEAT SINKS CONTAINING 50% PCM-50% METAL FOAM COMPARED TO A PCM HEAT SINK WITH NO
FOAM AND A CONVENTIONAL HEAT SINK WITHOUT PCM

Heat sink configurations	No PCM	PCM, no foam	1664 cells	25 990 cells	207 940 cells
PCM begins to melt at	–	14.5 s	7.2 s	5.5 s	5.2 s
PCM molten at	–	116.8 s	46.3 s	31.4 s	28.5 s
Temperature at $t = 10$ s	56.4 °C	54.8 °C	54.2 °C	53.8 °C	53.5 °C
Temperature at $t = 20$ s	63.4 °C	61.0 °C	58.9 °C	56.3 °C	55.3 °C
Temperature at $t = 30$ s	69.6 °C	66.4 °C	62.2 °C	57.8 °C	56.8 °C
Temperature at $t = 50$ s	80.6 °C	74.8 °C	66.7 °C	66.7 °C	66.7 °C
Temperature at $t = 70$ s	89.8 °C	81.0 °C	75.6 °C	76.1 °C	76.2 °C
Temperature at $t = 100$ s	101.0 °C	87.4 °C	88.0 °C	88.4 °C	88.5 °C
Temperature at $t = 200$ s	123.0 °C	110.7 °C	116.9 °C	117.1 °C	117.1 °C

TABLE VI

PARAMETERS OF THE STEP RESPONSES OF HEAT SINKS WITH 207 940 CELLS CONTAINING DIFFERING AMOUNTS OF
PCM COMPARED TO A PCM HEAT SINK WITH NO FOAM AND A CONVENTIONAL HEAT SINK WITHOUT PCM

Heat sink configurations	No PCM	PCM, no foam	35% PCM	50% PCM	85% PCM
Temperature at $t = 10$ s	56.4 °C	54.8 °C	53.5 °C	53.5 °C	53.5 °C
Temperature at $t = 20$ s	63.4 °C	61.0 °C	55.7 °C	55.3 °C	55.1 °C
Temperature at $t = 30$ s	69.6 °C	66.4 °C	59.2 °C	56.8 °C	56.1 °C
Temperature at $t = 50$ s	80.6 °C	74.8 °C	69.4 °C	66.7 °C	61.0 °C
Temperature at $t = 70$ s	89.8 °C	81.0 °C	78.5 °C	76.2 °C	71.1 °C
Temperature at $t = 100$ s	101.0 °C	87.4 °C	90.5 °C	88.5 °C	84.3 °C
Temperature at $t = 200$ s	123.0 °C	110.7 °C	118.0 °C	117.1 °C	114.9 °C

PCM foam cube size. For a foam which was selected to be approximately 50% PCM and 50% aluminium by volume, three cube sizes were compared: one with the outer cube having side length 1.15 mm, resulting in two planes in the 2.3 mm wide channel, giving approximately 1664 cells (cubes of Fig. 12) per heat sink channel; a second with side length 460 μm, resulting in five planes and approximately 25 990 cells per channel, and a third with cube side length 230 μm, producing ten planes and approximately 207 940 cells per channel. The latter is a realistic lower limit [15] for PCM foam. The heat sink is otherwise identical to that of Section IV (see Table II) and $c_{PCM} = 10$ mm. The step responses of heat sinks without PCM, with uniform PCM (no foam) and with the three different foam configurations to a 330 W step are shown in Fig. 16. The PCM temperature for the four heat sinks with PCM is given for the same step response is shown in Fig. 17. Clearly the foam structure causes the PCM to melt sooner; with the smallest cube size, the PCM begins to melt 5 s after the pulse is applied, as opposed to 14 s with the uniform (no foam) PCM. Also, the smaller the cell size and the finer the PCM-metal matrix, the sooner the PCM starts to melt – as expected, as the finer the matrix, the more high conductivity metal paths are present within the PCM to distribute heat more quickly. The same trend was seen when configurations with different proportions of PCM were simulated. The results are summarized in Table V. The sooner the PCM begins to melt, the sooner it melts completely, ending the temperature absorbing effect of the phase change. So while the foam causes the temperature reduction compared

to the heat sink without PCM sooner, the uniform, no foam PCM causes the temperature reduction to last longer. As seen in Table V, the temperature difference between the heat sink with PCM and the heat sink without at $t = 30$ s is as much as 13 °C for the PCM-metal foam, compared to only 3 °C for the uniform PCM, and at $t = 50$ s as much as 14 °C for the foam compared to 9 °C for the uniform PCM. However beyond those timescales, the uniform PCM performs better: there is only a 6 °C difference with the foam compared to 12 °C with the uniform PCM at $t = 200$ s for example.

Next, foam configurations with different amounts of PCM were examined. The results for foam containing 207 940 cells per channel with 35, 50, and 85% PCM are given in Fig. 18 and Table VI. The heat sinks with more PCM within the foam perform better, with the reduction in temperature compared to the conventional heat sink at $t = 50$ s being almost 20 °C for the foam with 85% PCM. Beyond $t = 100$ s all foam configurations again show the same trend, performing worse than the uniform PCM. In conclusion, for pulses in the range of minutes, such as those considered in Section IV, uniform PCM (no foam) remains the superior option. However for pulses from 30 s to 100 s in length, PCM-metal foam performs better than uniform PCM, particularly in the 30 to 50 s range where uniform PCM does not achieve a notable reduction in temperature. The use of PCM-metal foam allows hybrid PCM heat sinks to achieve the same type of performance in the 30 to 50 s range as is achieved with the uniform PCM in the minutes range.
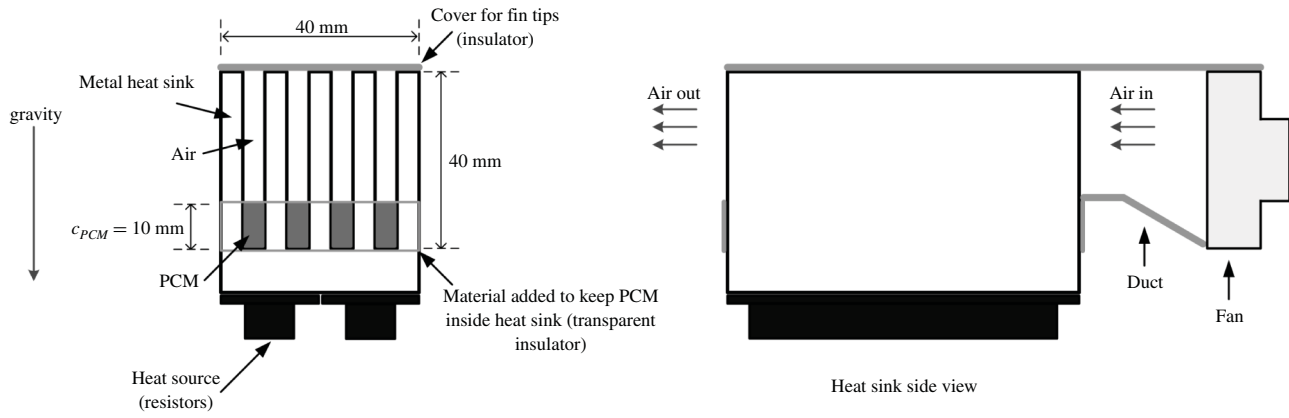
Fig. 19. Front and side view of the experimental setup.

b	c	L	n	s	t	d	c_{PCM}
40	40	80	16	1.4	1.0	10	10

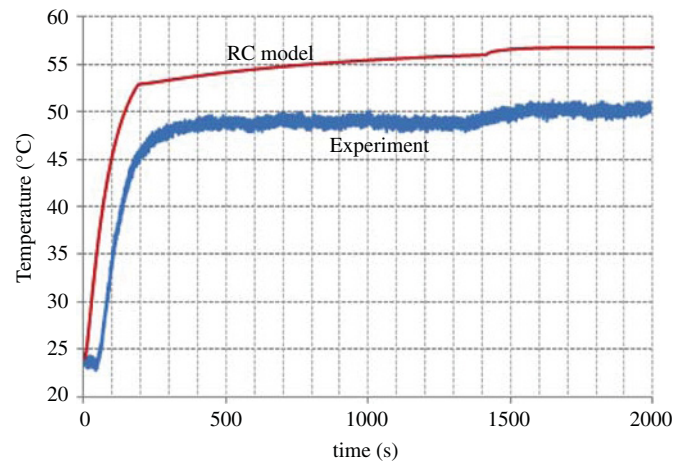| ρ kg/m^3	λ W/mK	ΔH kJ/kg	T_{melt} °C	C_p J/kgK
910	0.22	209.9	53	2220

Fig. 20. Temperature of the PCM inside the heat sink channels during a response to an 80 W step: experimental measurements versus the thermal network model's predictions. The thermocouple signal was RC-filtered before being connected directly into an oscilloscope channel without amplification. However, the effect of ambient noise is still visible in the measurements.

VI. EXPERIMENTAL RESULTS

For experimental verification of the model proposed in Section III, an existing aluminium heat sink optimized by the method of Section II for the Sanyo Denki *109P0412K3023* fan [19] was used. Specifications of the heat sink are given in Table VII. The heat sink was modified by adding *PlusICE A53*[22], an organic PCM similar in properties (see Table VIII) to the Suntech P116 material used in the previous sections. The configuration of the heat sink is as in Fig. 2, with $c_{PCM} = 10$ mm, and a duct constructed to direct all the air blown by the fan into the PCM-free portion of the fins. In the experiment, a constant heat of 80 W was applied via power resistors attached to the heat sink base plate. A sketch of the experimental setup is shown in Fig. 19. As the fan used is quite powerful, it was noticed during the experiment that the PCM was cooling quite quickly at its interface with the blowing air. Therefore, a resistor (similar to the ignored $R_{th,a}$ in Fig. 4) was added to the model of Fig. 7(b) between the midpoint of the PCM and the ambient to account for this heat transfer path. A standard K-thermocouple was used for temperature measurement. To avoid placing anything other than thermal paste between the resistors and the heat sink and for general ease of access, the thermocouple was inserted into the PCM itself between the channels, placed so that the tip of the sensor was approximately at the midpoint of the PCM block, and not touching the fins. The measured temperature

of the PCM in the experiment therefore corresponds to the temperature across capacitor $C_{th,PCM}$ in Fig. 7(b). The results of the experiment are given in Fig. 20, where the experimental measurements of the PCM temperature in the heat sink are compared with the temperature produced by the RC network model presented in this paper. As can be seen in Fig. 20, both curves, experimental and model, follow the same trend and have a very similar shape: fast heating up until the melting temperature (at about $t = 200$ s), then a much flatter portion as the PCM melts and then a "bump" (at about $t = 1400$ s) when the PCM is completely molten and as it heats up to reach the steady-state temperature. The experimental curve is flatter during the melting period than the simulated since in reality the PCM melts gradually, while in the model it is considered as one continuous block per channel that temperature of which changes uniformly at all points. However even with such a simplification, the shape of the simulated temperature matches well with the measurements. At steady state, there is a discrepancy of approximately 6 to 7 °C between the simulation and the measurement, which is in this case an

error of approximately 14% (57 °C max. temperature in the simulation versus 51 °C in the measurements). It must also be taken into consideration that the thermocouples used for measurement typically have an error of 2–4 °C. This is visible in Fig. 20, where the measurements show the PCM to begin melting at approximately 49 °C, while the PCM manufacturer gives the material's melting temperature as 53 °C (see Table VIII). Assuming such a measurement error of 4 °C, the error of the simulation reduces to about 2 to 4 °C or in this case approximately 8% at most. Therefore there is a good agreement between the model and real-world measurements, especially taking into account the model's relative simplicity.

VII. Conclusion

Hybrid heat sinks which are partially air-cooled and partially filled with PCMs offer a way to reduce the peak temperature amplitude in certain high peak load low duty cycle applications. Since the adding of PCM increases the thermal capacitance of the heat sink while also increasing its thermal resistance, care must be taken when selecting a heat sink configuration: the adding of PCM lowers the temperature only over a certain range of operation. Once the PCM has completely melted, the temperature eventually increases over that of a conventional heat sink. Furthermore, the utilization of the advantages of the PCM for each pulse requires complete re-solidification during the off-time. Therefore, the right configuration is strongly dependent on the application: the power pulse amplitude, period, and duty cycle.

In this paper, previous work on heat sink optimization was extended to create a thermal network model of a hybrid PCM heat sink. This allows for quick simulations of different heat sink configurations, so that an optimum design can be chosen. The optimization procedure presented in this paper is a good guide in selecting an optimum set of heat sink dimensions.

A conclusion can be also drawn about the general usefulness of the organic PCM materials typically studied in literature and examined in this paper: they do not melt quickly enough to be of significant benefit in situations where the pulses last only a minute or shorter. The use of such PCMs confers the most benefit in applications where the power pulsewidth is several minutes long and the period is measured in tens of minutes. In such applications, the peak temperature can be reduced by 10–20 °C, which is an improvement. To overcome this limitation, the concept of PCM-metal foam was explored: the foam forms a matrix of high conductivity metal paths in which the PCM is embedded, allowing for quicker melting of the PCM. As seen in Section V, a heat sink utilizing foam rather than uniform PCM can achieve the aforementioned temperature reduction with shorter pulses, in the 30 to 50 s range. However, it performs more poorly compared to the heat sink with uniform PCM with longer pulses.

Experiments have shown that the output of the thermal RC network model presented in this paper matches well with actual measurements. This confirms the usefulness of the model for designing and optimizing heat sinks with PCMs, especially considering its relative simplicity and much faster simulation time compared to e.g., 3-D-FEM.

References

[1] T. Wijekoon, L. Empringham, P. Wheeler, and J. Clare, "Compact dual-output power converter for an aerospace electrical landing gear actuation system," in *Proc. EPE*, Barcelona, Spain, Sep. 2009, pp. 1–10.

[2] *SINAUTEC Ultracap Bus Factsheet* [Online]. Available: http://www.sinautecus.com/products.html

[3] M. Ciappa, F. Carhognani, P. Cow, and W. Fichtner, "Lifetime prediction and design of reliability tests for high-power devices in automotive applications," *IEEE Trans. Device Mater. Rel.*, vol. 3, no. 4, pp. 191–196, Dec. 2003.

[4] M. Ciappa, "Lifetime prediction on the base of mission profiles," *Microelectron. Rel.*, vol. 45, nos. 9–11, pp. 1293–1298, 2005.

[5] J. Leland and G. Recktenwald, "Optimization of a phase change heat sink for extreme environments," in *Proc. 19th IEEE Semicond. Termal Meas. Manage. Symp.*, Mar. 2003, pp. 351–356.

[6] S. Krishnan, S. V. Garimella, and S. S. Kang, "A novel hybrid heat sink using phase change materials for transient thermal management of electronics," *IEEE Trans. Comp. Packag. Technol.*, vol. 28, no. 2, pp. 281–289, Jun. 2005.

[7] S. Krishnan and S. V. Garimella, "Analysis of a phase change energy storage system for pulsed power dissipation," *IEEE Trans. Comp. Packag. Technol.*, vol. 27, no. 1, pp. 191–199, Mar. 2004.

[8] B. Liu and P. Majumdar, "Numerical simulation of phase change heat transfer in PCM-encapsulated heat sinks," in *Proc. 18th IEEE Semicond. Termal Meas. Manage. Symp.* San Jose, CA, Aug. 2002, pp. 88–91.

[9] E. M. Alawadhi and C. Amon, "PCM thermal control unit for portable electronic devices: Experimental and numerical studies," *IEEE Trans. Comp. Packag. Technol.*, vol. 26, no. 1, pp. 116–125, Mar. 2003.

[10] U. Drofenik, G. Laimer, and J. W. Kolar, "Theoretical converter power density barriers for forced convection cooling," in *Proc. PCIM Europe*, Nuremberg, Germany, Jun. 2005, pp. 608–619.

[11] U. Drofenik and J. W. Kolar, "Analyzing the theoretical limits of forced air-cooling by employing advanced composite materials with thermal conductivities >400 W/mK," in *Proc. 4th Int. Conf. Integr. Power Syst.*, Naples, Italy, Jun. 2006, pp. 1–6.

[12] U. Drofenik, G. Laimer, and J. W. Kolar, "Pump characteristic based optimization of a direct water cooling system for a 10 kW/500 kHz vienna rectifier," *IEEE Trans. Power Electr.*, vol. 20, no. 3, pp. 704–714, May 2005.

[13] N. Zheng and R. A. Wirtz, "A hybrid thermal energy storage device, part I: Design methodology," *ASME J. Electron. Packag.*, vol. 126, no. 1, pp. 1–7, Mar. 2004.

[14] L. Huang, M. Petermann, and C. Doetsch, "Evaluation of paraffin/water emulsion as a phase change slurry for cooling applications," *Energy*, vol. 34, no. 9, pp. 1145–1155, Sep. 2009.

[15] P. A. E. Vallejos and C. Duston, "Carbon foam filled with phase change materials for passive temperature management," in *Proc. COMSOL Multiphys. User's Conf.*, Boston, MA, 2005, pp. 1–4.

[16] D.-W. Yoo and Y. K. Joshi, "Energy efficient thermal management of electronic components using solid-liquid phase change materials," *IEEE Trans. Device Mater. Rel.*, vol. 4, no. 4, pp. 641–649, Dec. 2004.

[17] V. Shanmugasundaram, J. R. Brown, and K. L. Yerkes, "Thermal management of high heat flux sources using phase change material: A design optimization procedure," in *Proc. 32nd Amer. Inst. Aeronaut. Astronaut. Thermophys. Conf.*, Atlanta, GA, Jun. 1997, pp. 1–10.

[18] V. S. S. Srinivas and G. K. Ananthasuresh, "Analysis and topology optimization of heat sinks with a phase-change material on COMSOL multiphysics platform," in *Proc. COMSOL Multiphys. User's Conf.*, Bangalore, India, 2006, pp. 1–7.

[19] *San Ace Cooling Systems*. Sanyo Denki S.A., Roissy Charles-de-Gaulle Cedex, France [Online]. Available: http://www.sanyodenki.eu

[20] S. Krishnan, J. Y. Murthy, and S. V. Garimella, "Analysis of solid-liquid phase change under pulsed heating," *ASME J. Heat Transfer*, vol. 129, no. 3, pp. 395–400, Mar. 2007.

[21] J.-J. Hwang, G.-J. Hwang, and C.-H. Chao, "Measurement of interstitial convective heat transfer and frictional drag for flow across metal foams," *ASME J. Heat Transfer*, vol. 124, no. 1, pp. 120–129, Feb. 2002.

[22] *Phase Change Materials: Thermal Management Solutions*. Phase Change Material Products Ltd., Hatfield, U.K. [Online]. Available: http://www.pcmproducts.net/

Andrija Stupar (S'02) was born in Belgrade, Serbia, in 1984. He received the Bachelors (with honors) and Masters degrees from the University of Toronto, Toronto, ON, Canada, where he worked on the design and implementation of digital controllers for low-power switch-mode power supplies. He is currently pursuing the Ph.D. degree with the Power Electronic Systems Laboratory, ETH Zürich, Zurich, Switzerland, with research focusing on modeling, simulation, and optimization of power converters.

Uwe Drofenik (S'96–M'00) was born in Mödling, Austria, in 1970. He received the M.Sc. (*cum laude*) and Ph.D. (*cum laude*) degrees in electrical engineering from the Vienna University of Technology, Vienna, Austria, in 1995 and 1999, respectively.

He was a Scientific Assistant with the Vienna University of Technology from 1997 to 2000, where he was involved in power electronic projects and computer-aided design/computer-aided manufacturing software development for industry. In 2001, he joined the Swiss Federal Institute of Technology Zürich, Zürich, Switzerland, as a Post-Doctoral Researcher, where he is heading the development of a multidisciplinary simulation software for virtual prototyping in power electronics. This includes the development, programming, and experimental testing of numerical circuit simulators, thermal and electromagnetic 3-D-finite element method simulators, algorithms for predicting reliability and life time of electronic components and systems, and the intelligent coupling of all these software-modules within a single design-platform. In 1996, he was a Researcher with the Masada-Ohsaki Laboratory, University of Tokyo, Tokyo, Japan. He is the author of the web-based interactive educational power-electronics software iPES. He has published more than 50 conference and journal papers and four patents.

Dr. Drofenik received the Isao Takahashi Award for Outstanding Achievement in Power Electronics from the IEE of Japan in 2005. He is a member of the Austrian Society of Electrical Engineering.

Johann W. Kolar (M'89–SM'04–F'10) received the M.Sc. and Ph.D. (*summa cum laude/promotio sub auspiciispraesidentisreipublicae*) degrees from the University of Technology Vienna, Vienna, Austria.

He has been an Independent International Consultant in close collaboration with the University of Technology Vienna since 1984, in the fields of power electronics, industrial electronics, and high performance drives. He has proposed numerous novel pulsewidth modulation converter topologies, and modulation and control concepts, e.g., the VIENNA rectifier and the three-phase AC-AC sparse matrix converter. He was appointed a Professor and Head of the Power Electronic Systems Laboratory, Swiss Federal Institute of Technology (ETH) Zürich, Zürich, Switzerland, in 2001. He has published over 350 scientific papers in international journals and conference proceedings and filed 75 patents. He initiated and/or is the Founder/Co-Founder of four spin-off companies targeting ultra-high speed drives, multidomain/level simulation, ultra-compact/efficient converter systems, and pulsed power/electronic energy processing. His current research interests include ac-ac and ac-dc converter topologies with low effects on the mains, power supply of data centers, more-electric-aircraft, distributed renewable energy systems, realization of ultra-compact and ultra-efficient converter modules employing latest power semiconductor technology (e.g. SiC), novel concepts for cooling and electro-magnetic interference filtering, multi-domain/scale modeling/simulation and multiobjective optimization, physical model-based lifetime prediction, pulsed power, and ultra-high speed and bearingless motors.

Dr. Kolar received the Best Transactions Paper Award from the IEEE Industrial Electronics Society in 2005, the Best Paper Award from ICPE in 2007, the First Prize Paper Award from IEEE IAS IPCC in 2008, the IEEE IECON Best Paper Award from IES PETC in 2009, the IEEE Power Electronics Society Transaction Prize Paper Award in 2009, and the Best Paper Award of the IEEE/ASME Transactions on Mechatronics in 2010. He received an Erskine Fellowship from the University of Canterbury, Christchurch, New Zealand, in 2003. In 2006, the European Power Supplies Manufacturers Association awarded him the Power Electronics Systems Laboratory, ETH Zürich, as the leading academic research institution in Power Electronics in Europe. He is an IEEJ member, and member of the international and steering committees and the technical program committees of numerous international conferences in the field of power electronics (e.g. Director of the Power Quality Branch of the International Conference on Power Conversion and Intelligent Motion). He is the founding Chairman of the IEEE PELS Austria and Switzerland Chapter and the Chairman of the Education Chapter of the EPE Association. From 1997 to 2000, he served as an Associate Editor of the IEEE TRANSACTIONS ON INDUSTRIAL ELECTRONICS. Since 2001, he has been an Associate Editor of the IEEE TRANSACTIONS ON POWER ELECTRONICS. Since 2002, he has also been an Associate Editor of the *Journal of Power Electronics* of the Korean Institute of Power Electronics and the Editorial Advisory Board Member of the IEEJ Transactions on Electrical and Electronic Engineering.